ACS APPLIED MATERIALS & INTERFACES
Research Article
www.acsami.org

Contribution to the Understanding of Capacity Fading in Graphene Nanosheets Acting as an Anode in Full Li-Ion Batteries

Óscar Vargas,[†] Álvaro Caballero,[†] Julián Morales,*[,†] and Enrique Rodríguez-Castellón[‡]

[†]Departamento Química Inorgánica. Instituto Universitario de Investigación en Química Fina y Nanoquímica. Universidad de Córdoba. 14071 Córdoba, Spain

[‡]Departamento de Química Inorgánica, Facultad de Ciencias, Campus de Teatinos, Universidad de Málaga, 29071 Málaga, Spain

S *Supporting Information*

ABSTRACT: Graphene nanosheets (GNS) were used as anodes in full Li-ion cells and $LiFePO_4$ (LFPO) was used as the cathode. A rapid decrease in capacity was observed following the first cycle, the origin of which was assigned to Li consumption in the solid-electrolyte interface (SEI) formation. A reduction of the irreversible capacity from 120 to a value as low as 20 mAh g^{-1}, similar to a commercial graphite anode, was possible through a prelithiation treatment prior to cell assembling. However, the GNS electrode barely delivered a capacity ca. 40 mAh g^{-1} at the end of cycle 50, notably lower than that of the graphite electrode (ca. 100 mAh g^{-1}). X-ray photoelectron spectroscopy spectra of the pristine electrodes at the end of 6th and 22nd charges, combined with depth profile analysis, supplied valuable information on the thickness and composition of the SEI. The spectra revealed that the SEI formed on the graphite electrode was much thicker than that formed on the GNS electrode and that its composition was controlled mainly by Li_2CO_3. The strength and the stability of Li_2CO_3 are two requisites for establishing a good SEI, which is the reason why the cell made from graphite performed better.

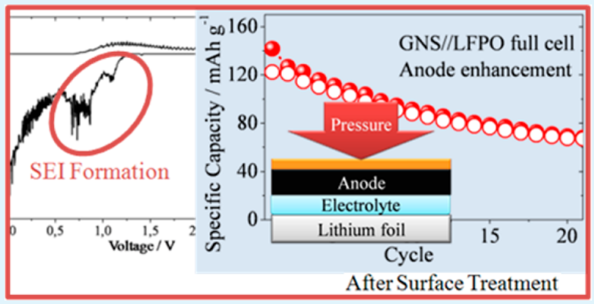

KEYWORDS: *li-ion batteries, graphene-based anode, full cell configuration, solid-electrolyte interface, anode prelithiation*

1. INTRODUCTION

Graphene nanosheets, as other graphene-based materials, have become a trendy topic in material science with several applications the subject of intensive research, and their use in Li-ion batteries (LIBs), also a booming research topic,[1−4] is no exception. The outstanding conductive properties and the possibility of storing Li^+ in both sides of the layer defects are attractive features when using these materials as anodes in Li ion batteries.[5−8] The electrochemical behavior of GNS in half cells (against Li metal) has been studied extensively with disparate results concerning their performance.[9−11] Recently, we applied different synthesis procedures (chemical reduction and thermal exfoliation of graphitic oxide) for obtaining GNS,[12] being the best performing material that synthesized with N_2H_4 as the reducing agent. The formed half cell exhibited high initial discharge (2665 mAh g^{-1}); however, it also showed very high initial irreversibility (1407 mAh g^{-1}), feature commonly found in this material.[12] Such a drawback results in a lack of the maintenance of capacity during cycling (it faded to 688 mAh g^{-1} at the 100th cycle). The irreversibility in the first discharge is attributed to the solid-electrolyte interface (SEI) formation.[13−15] This process consumes Li ions, leading to a decrease in the amount of Li available to be stored. In half cells, this is not a significant inconvenience because Li metal provides an abundant source of Li ions; however, it is a detrimental shortcoming for Li-ion batteries (full cell configuration) when Li metal is substituted by a Li-based compound as the electrode (usually Li spinels, Li-based layered oxides, or Li-based phosphates). High consumption of Li to form the SEI would exhaust the cathode material, resulting in capacity fading and shortening of the cycle life of the cell. A plausible solution to overcome this intrinsic problem is to generate the SEI on the anode surface before assembling the cell. The SEI formation can be implemented in two ways. It can be generated electrochemically, i.e., precycling the electrode with a Li foil as the counter electrode,[16,17] which is a time-consuming procedure because it must be performed at a low rate. The other method is through a surface treatment proposed by Hassoun et al.[18] and Liu et al.,[19] which consists of placing the electrode under a small pressure for some minutes in contact with a Li foil wetted with the electrolyte. This process is simpler and faster than the electrochemical procedure.

The above shortcomings could be one of the reasons explaining the copious literature reporting on the use of GNS as electrodes against Li, compared with their use in real Li-ion batteries (full cell configuration). To date, we have been unable to find any reference in the literature concerning the use of pure graphene in this configuration. Recently, we reported a preliminary study using the $LiNi_{0.5}Mn_{1.5}O_4$ spinel as the cathode.[20] The cell made from the GNS electrode without

Received: November 19, 2013
Accepted: February 12, 2014
Published: February 12, 2014

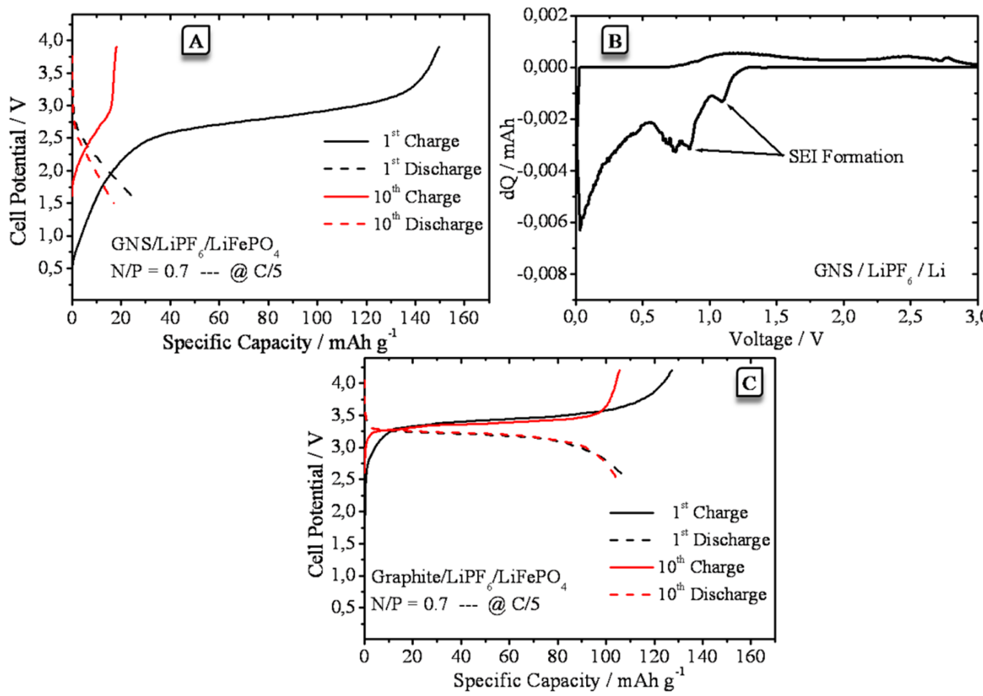

Figure 1. (A) Charge and discharge curves for the cell made from the pristine GNS and LFPO. (B) PCGA of the pristine GNS electrode vs. Li foil. (C) Charge and discharge curves for the cell made from graphite and LFPO.

any pre-activation failed in the first few cycles. A better electrochemical response was obtained with the electrode activated electrochemically, but the average capacity delivered by the cell, around 100 mAh g^{-1}, was maintained during the first ten cycles only, and then the capacity faded with celerity. In addition to the irreversible capacity of the graphene electrode, the spinel itself is not ruled out, among the other factors, for causing this unwanted behavior, because the high potential required for the Li ion release may decompose the electrolyte.[21]

In this paper, we shed light on the electrochemical behavior of GNS in a real LIB. To ensure the stability of the electrolyte, the spinel electrode was changed to an electrode made from commercial LFPO, which does not require such a high working potential, and the polarization between the charge and discharge curves is lower.[22−24] In either case, the interaction between the GNS and the electrolyte plays a key role in the cell operation. X-ray photoelectron spectroscopy (XPS) is one of the best tools for analyzing the SEI structure,[13,25] which is composed of a complex matrix of organic and inorganic compounds with a thickness of up to ∼800 Å.[26] This technique provides very valuable information on the chemical environment of the elements for identifying the functional groups that participate in the SEI framework. Moreover, by making use of the depth profile analysis, the spectra evolution with etching time provides relevant information both of its composition and its thickness. A full cell made from commercial graphite as the anode and commercial LFPO as the cathode was also studied for comparison.

2. EXPERIMENTAL SECTION

Materials. The GNS employed in this study were made of the same material synthesized and characterized elsewhere.[12] In short, it was prepared by the reduction of graphene oxide with 1 M N_2H_4 aqueous solution at reflux over 6 h. The nanosheets exhibited the common features of this kind of graphene-based material. It is disordered carbon (wide peak at ∼24° in 2θ, as revealed by X-ray diffraction) with high surface disorder, as measured by Raman spectroscopy (D to G bands intensity ratio of 0.91), and with the typical morphology of very thin and wrinkled sheets (studied by transmission electron microscopy). The cathode material was commercial $LiFePO_4$ (LFPO) supplied by Phostech Ltd. with a 2.1% carbon coating. To compare the electrochemical performance of GNS with graphite, the anode material used commonly in commercial LIBs, a commercial graphite electrode supplied by the MTI Corporation was used in combination with LFPO.

Electrochemical Measurements. The electrodes of GNS were prepared as reported elsewhere,[12] i.e., deposited by "doctor blade" on Cu foil in weight proportion of 85:15:5 referring to GNS:PVDF binder: carbon Super P, respectively. The cathode was prepared in weight proportion 80:10:10 referring to LFPO:PVDF:carbon Super P, respectively. This mixture was treated with 1-methyl-2-pyrrolidinone (Sigma-Aldrich) to obtain a slurry that was then deposited on an Al foil by the "doctor blade" technique. All the electrochemical tests were performed in Swagelok-type cells and using as electrolyte 1M $LiPF_6$ salt dissolved in a 1:1 (w/w) mixture of ethylene carbonate (EC) and dimethylcarbonate (DMC). Galvanostatic measurements were performed in two different configurations: the half cell configuration in which the working electrode is assembled with a Li foil as the counter electrode, and the full cell configuration in which the GNS or the graphite is confronted to a LFPO cathode. The half cells were cycled at $C/5$ with C as the theoretical capacity of the electrode material, i.e., 744 mAh g^{-1} for GNS, 372 mAh g^{-1} for graphite, and 170 mAh g^{-1} for LFPO; the voltage windows were: 3.0−0.01 V for GNS, 2.0−0.01 V for graphite, and 2.5−3.9 V for LFPO. Taking into account that the cathode material is often the most expensive part of the battery, the full cells should be mass balanced in order to reduced the cathode content, such balance is made according to the anode to cathode average capacity ratios (N/P), calculated by using the eq 1, recommended values of N/P for commercial batteries are close to 1.

$$\frac{\mathrm{N}}{\mathrm{P}} = \frac{C_{\mathrm{AV.An}} M_{\mathrm{An}}}{C_{\mathrm{AV.Cat}} M_{\mathrm{Cat}}} \tag{1}$$

N/P ratios of 0.7 and 1.0 have been used in this study, taking as average capacities: 600 mAh g^{-1} for GNS ($C_{\mathrm{AV.An}}$), 250 mAh g^{-1} for

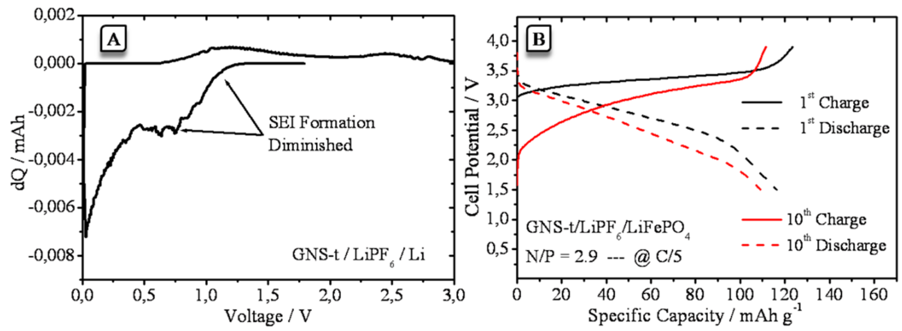

Figure 2. (A) PCGA of the GNS-t electrode vs. Li foil. (B) Charge and discharge curves for the cell made from GNS-t and LFPO.

graphite ($C_{AV.An}$), and 140 mAh g^{-1} for LFPO ($C_{AV.Cat}$). The full cells were cycled at C/5 referring to the cathode mass (M_{Cat}), regardless of the anode mass (M_{An}) being used, i.e., a current intensity of 34 mA g^{-1}. To improve the electrochemical performance of the GNS, the electrode was prelithiated in contact with a Li foil soaked in electrolyte, under a pressure of ca. 1 kg cm^{-1} for 5 min. The so treated electrode was labeled GNS-t. All the galvanostatic measurements were performed on an Arbin BT2000 potentiostat−galvanostat system. To test the effect of the surface treatment, we performed the potentiodynamic cycling with galvanostatic acceleration (PCGA) to the pristine and prelithiated GNS-based electrodes on a VMP-Biologic Science instrument in the voltage window of 3−0.01 V with 10 mV step potential and limit current of 15 μA. For the test, the electrodes were assembled in a three-electrode cell with Li foil as the reference and counter electrode, i.e., a half cell configuration.

XPS Analysis of SEI. To analyze the surface of the electrodes by XPS, we selected eight samples: the pristine electrodes (GNS and graphite), both electrodes after surface treatment, both electrodes after the 6th charge, and both electrodes after 22nd charge. The cycled electrodes were collected after disassembling the cells inside the glovebox. All samples were soaked in DMC to remove soluble species and then dried inside the glovebox under vacuum; the dried samples were collected in an Eppendorf vessel and sealed for transfer to the XPS instrument. XPS spectra were obtained on a Physical Electronics PHI 5700 spectrometer using non-monochromatic Mg Kα radiation (300 W, 15 kV, 1253.6 eV) and a multi-channel detector. Spectra for the samples were recorded in the constant pass energy mode at 29.35 eV, using a 720 μm diameter analysis area. Binding energy (BE) values were referred to the C 1*s* peak at 284.8 eV. The CA PHI ACCESS ESCA-V6.0 F software package was used for data acquisition and processing. A Shirley-type background was subtracted from all signals. Recorded spectra were always fitted using Gauss-Lorentz curves to determine more accurately the binding energy of the different element core levels. The error in BE was estimated to be ca. ±0.1 eV. An Ar^+ ion beam of 4 keV was used for depth profiling, and compositions were determined from the integrated intensities of the XPS spectra.

3. RESULTS AND DISCUSSION

3.1. Cycling Performance. Full cells, assembled with GNS as the anode and commercial LFPO as the cathode, were cycled at C/5 rate, referring to the cathode mass with different anode to cathode average capacity ratios, named N/P 0.7 and 1.0. The following arguments justify the selection of these two values. The first is based on different reports where a slight excess of cathode material ensures the carbon acts as the limiting electrode and the second is based on the ideal proportions.[27] Figure 1A shows the charge/discharge curves for the 1st and 10th cycles for the cell made with an N/P ratio of 0.7. The first charge curve exhibits a pseudo-plateau from 2.3 to 3.2 V centered around 2.6 V. The shape of the charge curve shows the characteristic plateau at 3.5 V[22−24] observed for LFPO in half cells (see Figure S1A in the Supporting Information), but with a lower polarization at the start of the process, which resembles the charging behavior of GNS (see Figure S1B in the Supporting Information). The capacity was around 150 mAh g^{-1}, somewhat higher than the average obtained from a half cell. The first discharge exhibited a highly polarized curve, the shape of which is more similar to that observed for GNS in the half cell configuration (see Figure S1B in the Supporting Information). However, more striking was the reduced delivered capacity, which was slightly above 20 mAh g^{-1}. The irreversible capacity should be associated with the SEI formation, typical of carbonaceous anodes.[13,26] This causes a continuous degradation in the cell performance, as observed in Figure 1A and Figure S2 in the Supporting Information, where the discharge capacity values are plotted as a function of the number of cycles. This figure also shows the performance of the cell for an N/P ratio of close to 1. The delivered capacity with this ratio was lower, behavior which was also found for other cells as shown below.

To shed additional light on the SEI formation, the PCGA curves were recorded for the pristine GNS anode vs. Li foil (Figure 1B). The discharge curve shows an intense and wide peak at around 0.8 V, which is assigned to the electrolyte decomposition in carbonaceous anodes.[13,26] It also shows a smaller peak at a higher potential (ca. 1.1 V), the origin of which is not known, but it reflects a certain divergence of the electrochemical behavior of graphene compared with other carbonaceous materials. The charge curve shows two weak and broad peaks at ca. 1.2 and 2.5 V (this latter somewhat weaker). The lower voltage peak is assigned to the release of lithium intercalated in the GNS. The higher voltage peak is assigned to the SEI decomposition, consistent with the statement of Winter et al. regarding to the SEI reversibility; the SEI formation on negative electrodes in organic electrolytes is generally irreversible but, under certain charge/discharge conditions SEI may be removed.[15] This observation is relevant in the context of the global article content. As shown below the full cells made from GNS and LFPO were cycled down to 1.5 V. By assuming that LFPO remains at 3.5 V vs. Li/Li^+, the GNS reaches to 2.0 V vs. Li/Li^+. In other words, the GNS electrode is below the SEI decomposition potential and, as a result, the SEI is maintained electrochemically stable during cycling. For comparison, a full cell using commercial graphite with an N/P ratio of 0.7 is shown in Figure 1C. The charge curve shows a short polarization and a well-defined plateau at ca. 3.3 V, as expected from the curves of these two materials in the half cells[22−24] (see Figure S1A and C in the Supporting Information). The charge capacity value was 130 mAh g^{-1}, which is somewhat lower than that of the GNS-based cell, because of the differences in the cell polarizations at the beginning of the process. Moreover, the shape of the discharge curve also shows the expected plateau taking into account the electrochemical behavior of the two components against Li. The delivered capacity was around 110 mAh g^{-1}, a value somewhat lower than that of the charge. Nevertheless, the irreversible capacity of this cell was notably lower than that of the GNS cell. This feature has beneficial effects for cell performance. On further cycling, the shapes of the curves do not undergo significant changes and the maintenance of the capacity with cycling is much better than that of cell made from GNS.

The poor electrochemical response of the GNS electrode in full cells is a significant obstacle to its application in practical batteries. The reduction of the initial irreversible capacity might be an appropriate strategy to improve its performance. For this end, we implemented a surface treatment to produce an SEI ex situ and to diminish the amount of Li irreversibly consumed in this process during cycling. The method chosen was the easiest,[18,19] which consists of placing the electrode, under a small pressure for some minutes, in contact with a Li foil wetted with the electrolyte. The effectiveness of this treatment to generate the SEI is shown in the PCGA curve of Figure 2A. The intensity of the wide peak at ca. 0.8 V decreased and the small peak observed in Figure 1B at 1.1 V was suppressed, which provides evidence of its origin related to the SEI formation. On the other hand, Figure S3 in the Supporting Information shows that the initial irreversible capacity was reduced notably from 963 mAh g^{-1} for the pristine GNS electrode to196 mAh g^{-} after its prelithiation, as evaluated from the half cell configuration. Moreover, the irreversible capacity was also reduced on further cycles.

Figure 2B shows the charge and discharge curves of the full cell assembled with GNS-t and LFPO at an N/P ratio of 0.7. The main difference between the first charge curve and that of Figure 1A is the higher open-circuit voltage due to the prelithiation process. The capacity value was ca. 140 mAh g^{-}, which is somewhat lower than the cell made with untreated GNS (see Figure 1A). The discharge curve starts with a short plateau (as observed for LFPO vs. Li, Figure S1A in the Supporting Information), followed by a smooth and continuous fall of potential as the process progresses (as observed for GNS vs. Li, see Figure S1B in the Supporting Information). The delivered capacity increased notably, to ca. 122 mAh g^{-1}. This lower irreversible capacity improved the electrochemical response of the cell and at the 10th cycle, the delivered capacity was ca. 90 mAh g^{-1}.

The cycling behaviors of the full cells assembled with GNS-t as the anode and commercial LFPO as the cathode for N/P ratios of 0.7 and 1.0, cycled at C/5 rate are shown in Figure 3. Although the performances of both cells improved clearly compared with that of the cells made from pristine GNS (see Figure S2 in the Supporting Information), the delivered capacity faded with cycling. The tendency was to improve the capacity retention as the cycle number increased. The best performance was obtained for the cell with an N/P ratio of 0.7, the capacity of which at the 50th cycle was 40 mAh g^{-1}. Also, the initial irreversibility was removed almost completely with the prelithiation treatment. The cycling properties of two full cells made from graphite and LFPO and identical N/P ratios have also been included for comparison. The first charge and discharge capacity of these cells were rather similar, ca. 130 and 108 mAh g^{-1}, respectively. These values are comparable with those obtained in similar conditions by Amine et al.[24] On the other hand, the irreversible capacity of both cells was very

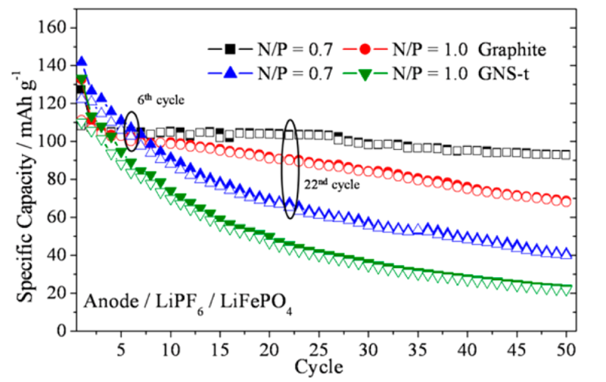

Figure 3. Comparison of the cycling behavior of GNS-t and graphite full cells made with two different N/P ratios. The cells were cycled at C/5, referring to LFPO. The empty and full symbols correspond to charge and discharge values, respectively.

similar to that of the cells made with GNS-t, additional proof of the role played on the irreversible capacity by the prelithiation process. At the end of the 50th cycle, the discharge capacity of the cell with an N/P of 0.7 faded to 86% of its initial value, and that with an N/P ratio of 1.0 fell to 53%. Again, an increase in the ratio produces a poorer performance. With regard to the influence of the anodic material, GNS-t provided poorer results than graphite did, regardless of the N/P ratio. To establish a satisfactory explanation for this different behavior, we recorded the XPS spectra of the electrodes submitted to different charge/discharge processes. The results of these measurements are discussed in the next section.

3.2. XPS Analysis of the SEI. As commented above, the prelithiation treatment was implemented to diminish the initial irreversible capacity, the origin of which is associated with the decomposition of the electrolyte and SEI formation.[13−15] However, this treatment was insufficient to maintain an optimal performance of the cell during prolonged cycling. SEI is formed mainly in the first cycle. Nevertheless, the SEI formation is far from being a static phenomenon; on the contrary, it is a dynamic process that changes continuously both in extent and composition from one cycle to another.[26] This is a plausible way to explain the differences in the capacity retention between the GNS-t and graphite cells. The dynamics involved in both cells should be different, such that the irreversible consumption of Li in the GNS-t cell would be extended throughout the entire cycling, leading to a greater extent of capacity fading compared with the graphite cell.

Figure 4 shows the XPS spectra for pristine GNS and graphite electrodes (without prelithiation or cycling treatments). At first sight, there are remarkable differences in the C 1s and O 1s spectra of both electrodes. The C 1*s* spectra exhibit peaks from 286 to 289 eV, which correspond to the oxygenated functional groups (C−OH, C−O−C, C═O, O−C−O, and O═C−O). For GNS, these oxygenated groups probably belong to groups not removed from the graphitic oxide, whereas in the graphite electrode, the oxygenated groups belong to the carboxymethyl cellulose (CMC) binder. The peaks at 284.9 (GNS) and 285.0 eV (graphite) are due to the carbon framework of the electrodes (together with adventitious carbon). The lower content of this component for graphite can be explained by assuming a high concentration of CMC at the surface level. The peaks of the GNS electrode at 286.0 and 287.3 eV are assigned, partially, to C bound to N, $C-NH_2$ and C−NH, respectively, the origin of which is due to the synthesis

dx.doi.org/10.1021/am405197s | ACS Appl. Mater. Interfaces 2014, 6, 3290−3298

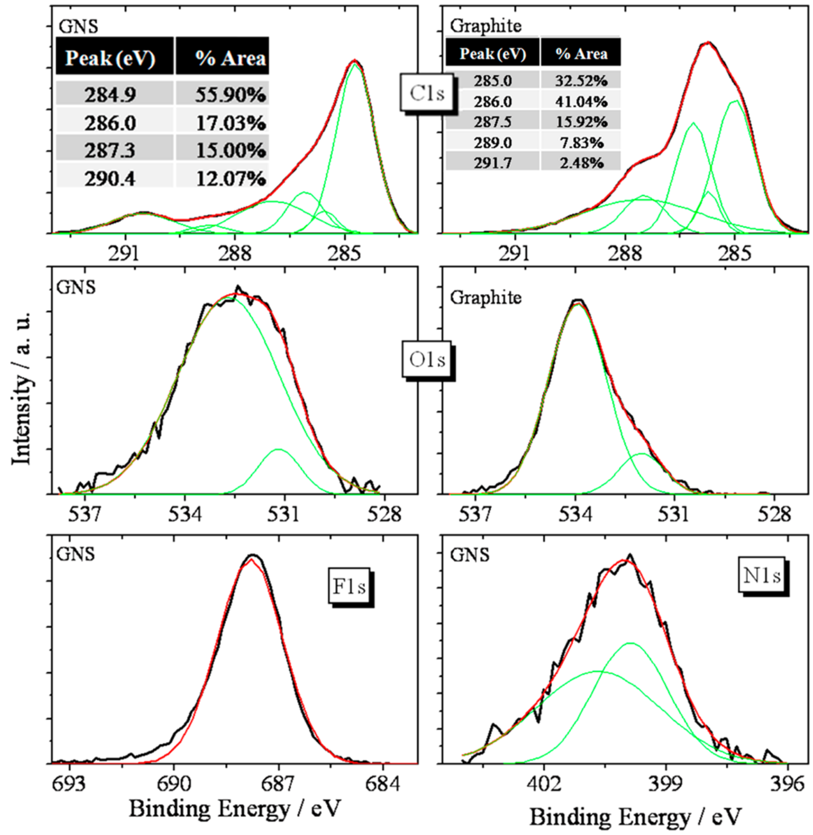

Figure 4. C 1s, O 1s, N 1s, and F 1s spectra for the GNS electrode, and C 1s and O 1s spectra for the graphite electrode.

with N_2H_4.[28−30] Regarding the N 1s, the spectrum was fitted to two components centered at 399.9 and 400.7 eV, corresponding to pyrrolic (44.33 %) and graphitic (55.67 %) nitrogen.[30] The O 1*s* peaks of graphite at 532.3 and 534.0 eV are assigned to the cellulose of CMC binder. The O 1*s* spectrum of GNS exhibit peaks at 531.5 (C═O) and 533.4 eV (C−OH), these peaks are assigned to the remaining functional groups from graphitic oxide.[31] It is worth it to note that in GNS there are similar contents of C═O (54.03 %) and C−OH (45.97 %) such similarity is also observed in the C 1s spectra with the corresponding assignations to C−OH/C−O−C (17.03 % at 286.0 eV) and C═O/O−C−O (15.00 % at 287.3 eV). The higher energy peak observed at 290.4 eV in the C 1s spectrum for GNS, corresponds to $C-F_2$ bonds of the PVDF binder; this was confirmed by the F 1s peak at 687.8 eV.[13,32] The weak peak at 291.7 eV in the graphite electrode is probably due to graphitic shake up (π to π^* transition).[31]

As expected, the graphite electrode is composed only of C and O, whereas the GNS electrode is a more complex matrix due to the presence of F from the PVDF binder and N derived from the synthesis method. Table 1 shows the composition of both electrodes. There are some discrepancies between the content of PVDF and CMC binders calculated from these values and those used for preparing the electrodes. XPS spectra lead to a higher content. Regardless, these differences can be explained by taking into account that the XPS technique analyzes the surface composition and the PVDF binder tends to coat the active particles, as revealed by Lee et al. from SEM images.[32] It is not ruled out that CMC might also tend to be localized on the surface.

Table 1. Chemical Composition of the Pristine Electrodes Calculated from XPS Spectra

atomic %	pristine GNS	pristine graphite
C 1s	76.31	81.99
O 1s	9.47	17.71
F 1s	10.70	0
N 1s	3.42	0

3.3. Prelithiation of GNS. Figure 5 shows the C 1s, O 1s, and F 1s spectra of the GNS-t. For comparison, graphite was also prelithiated with the same procedure and the spectra of these elements are shown in Figure S4 in the Supporting Information. Both C 1s spectra were fitted to three components assigned to C−C and/or C−H at 284.8 eV, polymers and alkyl groups C═O at ca. 286 eV and Li_2CO_3 and, for GNS-t only, $-CF_2-$ at ca. 290.0 eV. For the GNS-t sample, the carbon content assigned to carbonate was higher than that referred to C−C (54.21 % vs. 43.79 %); for graphite, the contents were similar (49.72% and 47.41%), in both cases polymers and alkyl carbonates were lower than 3%. Although the O 1*s* spectra showed a similar shape to those belonging to the pristine electrodes (Figure 4), also fitted to two components, a significant alteration was observed in their relative intensities. The prelithiation process clearly increased the intensity of the lower energy peak at ca. 532.0 eV, commonly assigned to Li_2CO_3.[13,26] The F 1s spectrum of the GNS-t electrode clearly underwent significant alterations because the single peak observed for the electrode made from GNS (Figure 4) was split into two components at 684.6 and 687.7 eV, the former somewhat less intense (43.81%) than the latter (56.19 %). The lower energy peak was assigned to LiF and the higher energy peak to the F of the PVDF component.[13,26] These two

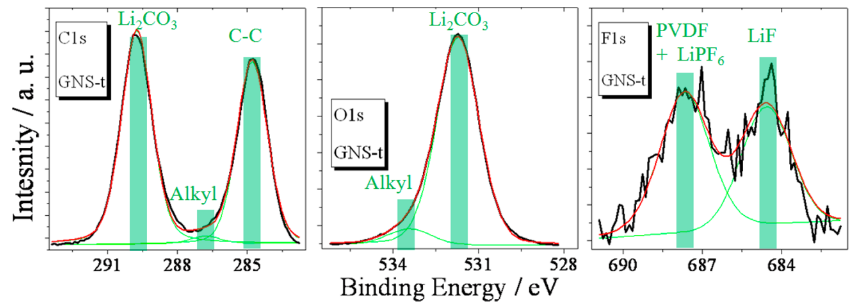

Figure 5. C 1s, O 1s, and F 1s XPS spectra for GNS-t.

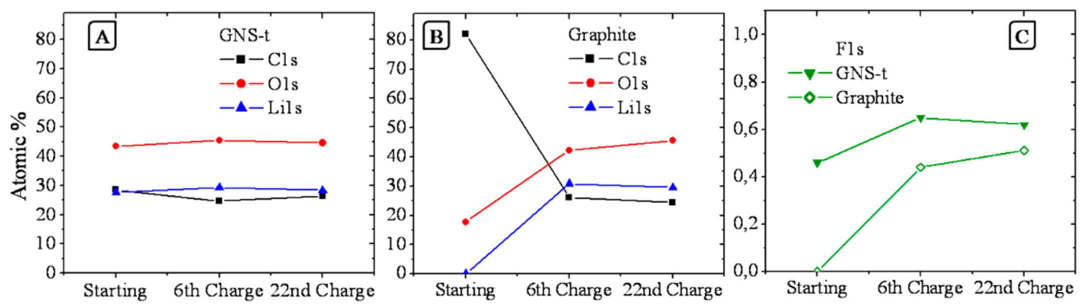

Figure 6. Atomic percentage of the C 1s, O 1s, and Li 1s for (A) GNS-t, and (B) pristine graphite. (C) F 1*s* atomic percentage. The different states of charge are referred to full cells.

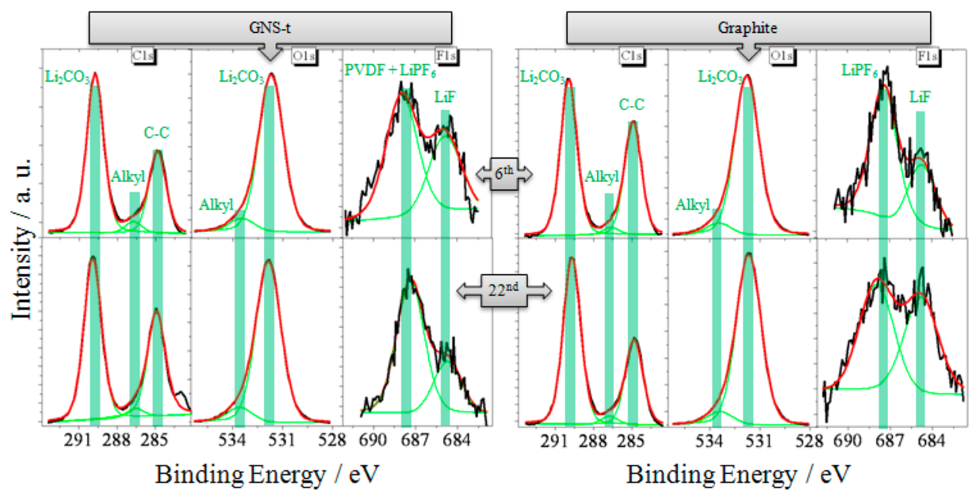

Figure 7. XPS C 1s, O 1s, and F 1s spectra for the GNS-t and graphite electrodes at the end of 6th and 22nd charges in full cells with LFPO as cathode.

components were also observed for the prelithiated graphite (see Figure S4 in the Supporting Information), where the lower energy peak was more intense (57.56 %). The origin of the higher energy peak is unclear because the binder of this electrode is not PVDF. One plausible explanation should be based on the Edström et al. who demonstrated that $LiPF_6$ can also contribute to this photoemission peak.[33] In our case, this salt could be present as an impurity in spite of the electrode was rinsed with DMC to remove it. An alternative explanation based on the PF_6^- anion located in the interlayer spacing of graphite described by Seel and Dahn[34] is unlikely, because this process happens when graphite is polarized above 4.5−-4.8 vs. Li/Li^+, a value notably exceeding the potential experienced by our anodes. As a final conclusion, the SEI formation, by means of the contact treatment, is clearly demonstrated by the presence of Li_2CO_3 and LiF.

3.4. SEI Evolution on Cycling. Figure 6 shows the atomic percentage of the GNS-t and graphite electrodes at different states of cycling. The starting state for the GNS-t electrode is the prelithiated material and for graphite, it is the pristine electrode (the prelithiated electrode was not used in a full cell configuration). Hence, the differences in the amount of the measured elements: C, O, Li, and F at the start. At the 6th charge, the amounts measured for the two electrodes were very similar (ca. 25 % C 1s, 43 % O 1s, and 30 % Li 1s, see Figure 6A, B). Taking into consideration that the carbon-based electrodes were discharged (while the cathode is charged in the full cell), part of this Li should be intercalated in the interlayer; the remainder should participate in the SEI framework. On the other hand, the contents of these elements hardly changed at the 22nd charge. As regards the F values, the GNS-t electrode (Figure 6C) always exhibited a higher content, which was due

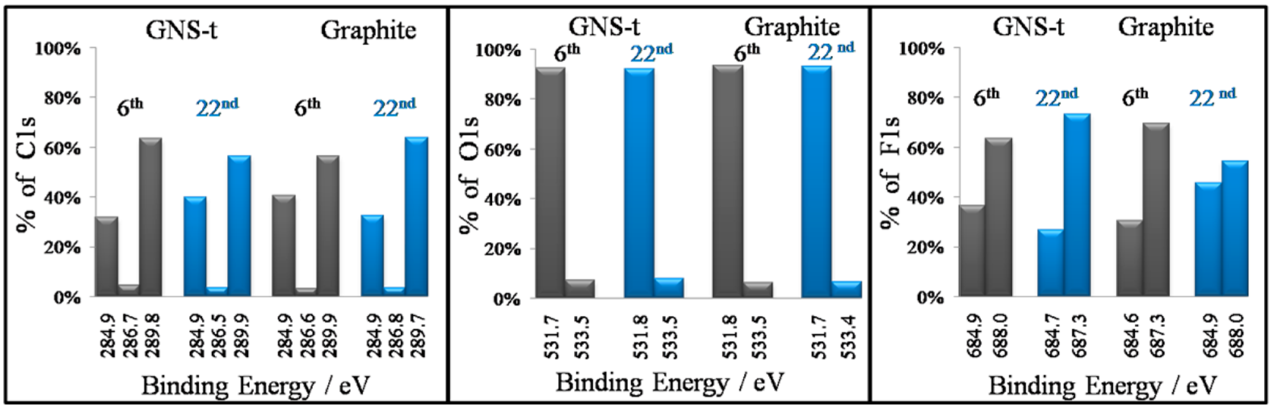

Figure 8. Quantities of C 1s, O 1s, and F 1s components calculated for the GNS-t and graphite electrodes at the end of 6th and 22nd charges in full cells with LFPO as the cathode.

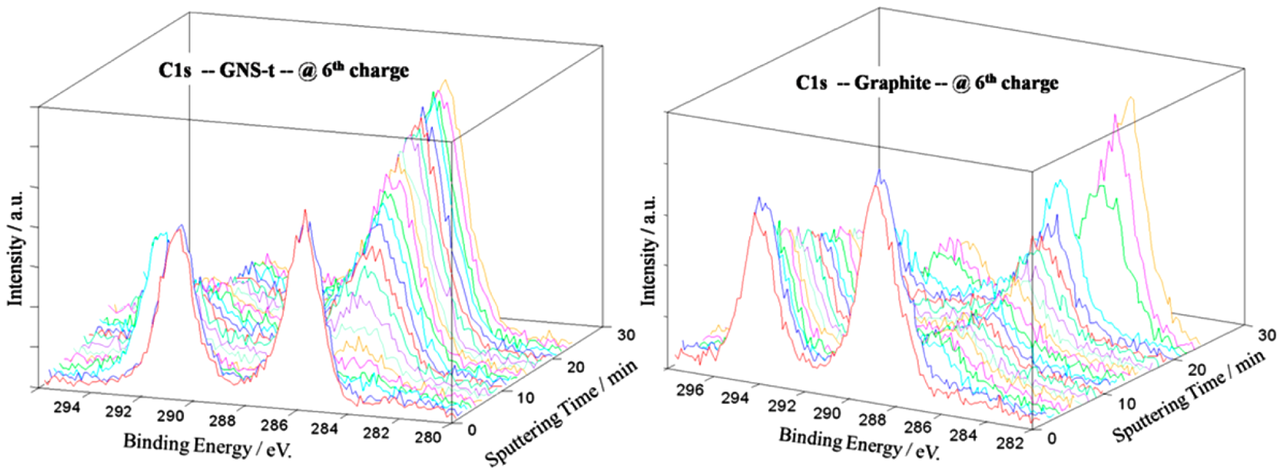

Figure 9. Depth profiles of the C 1s spectra after the 6th charge for the GNS-t and graphite electrodes.

in part to the initial content of PVDF and to the prelithiation treatment. However, at the 6th and 22nd charges, the uptake of F by the graphite electrode was higher, which corroborates the relevance of decomposition products coming from the electrolyte on this electrode. In addition to these differences between the two electrodes, the evolution of the different chemical environments could vary as a result of the cell operation. This information could be valuable in shedding light on the differences in SEI structure and in explaining the different electrochemical behaviors of the two electrodes.

Figure 7 shows the corresponding C 1s, O 1s, and F 1s spectra for the GNS-t and graphite electrodes, at the end of the 6th and 22nd charges. The shapes of the spectra are quite similar to those of Figure 5 and Figure S4 in the Supporting Information, and they were fitted to the same components.

The differences between the intensities of the different components of the spectra of Figure 7 are seen more clearly in the bars of Figure 8, which quantify the percentage of each component. The following comments describe the changes undergone by the spectra between the 6th and 22nd charges. For the C 1*s* spectra corresponding to GNS-t, the intensity of the peak at 284.9 eV increased from 31.87 to 39.89%; by contrast, the intensity of this peak for the graphite electrode decreased (from 40.57 to 32.62%). Taking into account that the lower the intensity of this peak, the thicker the SEI is,[23,32,35] the thickness of the SEI of the GNS-t electrode diminishes whereas that of the graphite electrode becomes thicker. In both cases, the change in thickness is accompanied by an opposite change in Li_2CO_3 content as revealed by the C 1s spectrum; nevertheless, these changes are not reflected in the intensities of the two peaks of O 1*s* spectrum. On the other hand, the changes in intensity observed for the peak at 284.9 eV on charging the cell (for the GNS-t electrode, from 43.79 after prelithiation to 31.87 % at the 6th charge) suggest an increase in the SEI thickness. The signal F 1s also showed differences. Thus, whereas the content of LiF in the GNS-t was reduced, it increased in the case of the graphite electrode. For the GNS-t electrode, the LiF content decreased upon cycling (from 43.81 % after the prelithiation process to 36.46% after cycling until the 6th charge and down to 26.81% at the end of the 22nd charge). This could be one of the reasons for the capacity fading. By adding LiF nanoparticles to a graphene electrode, Wu et al. established that for good performance, LiF is a key component of the SEI because it suppresses side reactions that affect the formation of organic components.[36] However, in our case, the formation of these organic components occurs simultaneously with LiF formation through the prelithiation treatment, and the possible positive effects of LiF are less defined.

The SEI of the GNS-t electrode formed at the 6th charge seems to be thicker than that formed on the graphite electrode, because the content of C 1*s* at ca. 285 eV is higher for the GNS-t than that corresponding to the graphite electrode (31.87% vs. 40.57%). However, as the electrodes are different in composition and structure, the processes related to SEI formation could be different. To shed light on this question, we ran a depth profile analysis at the 6th charge for both electrodes. The C 1s spectra of the depth profiles for both electrodes, presented in Figure 9, show a common feature; in the first minutes of sputtering, there is a pronounced decay of the peak at the lower binding energy. By contrast, the peak at the higher energy decays slowly. Moreover, the peak at the lower energy starts to reappear, increasing in intensity with sputtering time. The peak at the lower energy is a contribution from two components: lithium alkyl carbonates (at ca. 286 eV) and carbon/hydrocarbons (at ca. 285 eV). Under the sputtering treatment, the carbon and hydrocarbons could produce CO_2 and lithium alkyl carbonates react with CO_2 to produce Li_2CO_3.[13] This could be one plausible explanation for the maintenance of the peak intensity assigned to Li_2CO_3 (that at high binding energy) at the beginning of the sputtering process, which is also supported by the increase of O and Li concentration (see Figure 10). As the sputtering process continues, the intensity of the low binding energy peak starts to increase, and this is faster for the GNS-t electrode. The higher binding energy peak behaved in an opposite sense; it tended to decrease in intensity, but the peak of the GNS-t electrode decreased faster than that of the graphite electrode (see Figure 9). Translated to C atomic concentration, the XPS technique detects a higher C content for the GNS-t electrode, the origin of which must be assigned mainly to the carbon framework of the electrode. These data suggest that the SEI of the graphite electrode is thicker than that of the GNS-t electrode, and that its composition is controlled by carbonate-based species. The evolution of O, Li, and F concentrations give additional support to this suggestion. The higher O and Li contents found in the graphite electrode are consistent with a greater presence of phases derived from the electrolyte decomposition, i.e., a thicker SEI. The greater F content and its increase with sputtering time, as observed for the GNS-t electrode, compared with the low F content for the graphite electrode is also consistent with this model. The ease of SEI removal for the GNS-t electrode because of its thinness allows for the detection of the PVDF binder used in the electrode conformation.

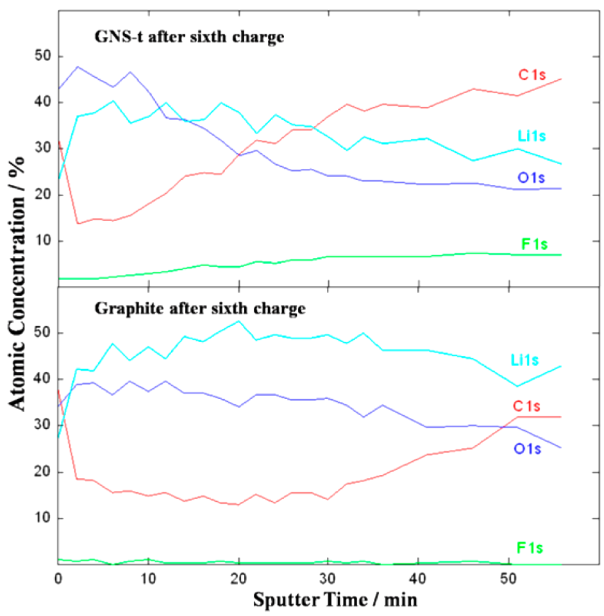

Figure 10. Atomic concentration extracted from depth profiles of the C 1s, O 1s, F 1s, and Li 1s spectra for the GNS-t and graphite electrodes after the 6th charge.

The relevance of the SEI on the negative electrode for good performance of the cell has been stated by different authors. According to Aurbach et al., it should contain stable and insoluble passivating agents such as Li_2CO_3 instead of Li-alkyl-based species, which are metastable and poor passivating agents.[37] The combination of XPS spectra with the depth profile analyses with Ar^+ revealed significant differences between the SEI structure of the GNS-t and graphite electrodes, which can be summarized by two principal observations: (i) a greater thickness of the SEI formed on the graphite electrode, and (ii) Li_2CO_3 is major component. These two properties of the graphite electrode could explain its better performance against $LiFePO_4$ (see Figure 3). This cell was able to maintain better capacity retention than the GNS-t electrode upon cycling. A very thin SEI, such as that inferred from XPS in the case of the GNS-t, is easily removed and the fresh electrode surface enhances side reactions, which are detrimental for good cell operation. A stronger and compact SEI hinders this shortcoming. Moreover, the prevalence of Li_2CO_3 in its composition assures SEI stability and thus, the cell performs better as a result.

4. CONCLUSIONS

GNS are unable to act as anodes in full LIBs with $LiFePO_4$ as the cathode material. The reason for this is their irreversible capacity observed in the first cycle vs. the Li electrode. This shortcoming can be mitigated by subjecting the electrode to a prelithiation treatment that facilitates SEI formation and reduces the irreversible Li^+ consumption. With this treatment, the electrochemical response of GNS electrodes in these Li-ion cells is comparable with that of graphite electrodes. However, on successive cycling, the cell made from GNS electrodes exhibits worse performance with poor capacity retention and faster capacity fading. XPS spectra revealed clear differences between the GNS and graphite electrodes regarding the thickness and composition of the SEI. The SEI formed on the GNS was very thin and its tendency to become thicker upon cycling is less than that on graphite. Furthermore, because upon Ar^+ sputtering the peak assigned to Li_2CO_3 disappeared faster in the GNS-t electrode than in the graphite electrode, the content of this inorganic salt is higher in the latter electrode. On the basis of these results, the poorer performance of Li-ion cells made from GNS is due to the thinness and deficiency in Li inorganic salts of the SEI formed on the GNS electrodes. A thicker SEI formed by insoluble passivating agents such as Li_2CO_3, characteristic of the SEI formed on the graphite electrode, accounts for a better electrochemical performance in Li-ion cells.

■ ASSOCIATED CONTENT

Supporting Information

Charge/discharge curves for half cells of LFPO, GNS, and graphite; cycling performance of GNS//LFPO full cells; cycling performance of GNS and GNS-t half cells; XPS spectra of prelithiated graphite. This material is available free of charge via the Internet at http://pubs.acs.org.

■ AUTHOR INFORMATION

Corresponding Author

*E-mail: iq1mopaj@uco.es. Tel.: +34 957218620.

Notes

The authors declare no competing financial interest.

ACKNOWLEDGMENTS

This work was performed with the financial support of the Ministerio de Ciencia e Innovación (Project MAT2008-03160 and MAT2011-27110) and Junta de Andalucía (Group FQM-175).

REFERENCES

(1) Bruce, P. G.; Scrosati, B.; Tarascon, J.-M. *Angew. Chem., Int. Ed.* **2008**, *47*, 2930.
(2) Tarascon, J.-M. *Philos. Trans. R. Soc., A* **2010**, *368*, 3227.
(3) Dunn, B.; Kamath, H.; Tarascon, J.-M. *Science* **2011**, *334*, 928.
(4) Choi, N.-S.; Chen, Z.; Freunberger, S. A.; Ji, X.; Sun, Y.-K.; Amine, K.; Yushin, G.; Nazar, L. F.; Cho, J.; Bruce, P. G. *Angew. Chem., Int. Ed.* **2012**, *51*, 9994.
(5) Yin, S.; Zhang, Y.; Kong, J.; Zou, C.; Li, C. M.; Lu, X.; Ma, J.; Boey, F. Y. C.; Chen, X. *ACS Nano* **2011**, *5*, 3831.
(6) Yoo, E. J.; Kim, J.; Hosono, E.; Zhou, H.; Kudo, T.; Honma, I. *Nano Lett.* **2008**, *8*, 2277.
(7) Zhu, Y.; Murali, S.; Cai, W.; Li, X.; Suk, J. W.; Potts, J. R.; Ruoff, R. S. *Adv. Mater.* **2010**, *22*, 3906.
(8) Pumera, M. *Energy Environ. Sci.* **2011**, *4*, 668.
(9) Abouimrane, A.; Compton, O. C.; Amine, K.; Nguyen, S. T. *J. Phys. Chem. C* **2010**, *114*, 12800.
(10) Pan, D.; Wang, S.; Zhao, B.; Wu, M.; Zhang, H.; Wang, Y.; Jiao, Z. *Chem. Mater.* **2009**, *21*, 3136.
(11) Yin, S.; Zhang, Y.; Kong, J.; Zou, C.; Li, C.M.; Lu, X.; Ma, J.; Boey, F. Y. C.; Chen, X. *ACS Nano* **2011**, *5*, 3831.
(12) Vargas, O. A.; Caballero, A.; Morales, J. *Nanoscale* **2012**, *4*, 2083.
(13) Verma, P.; Maire, P.; Novák, P. *Electrochim. Acta* **2010**, *55*, 6332.
(14) Hayner, C. M.; Zhao, X.; Kung, H. H. *Annu. Rev. Chem. Biomol. Eng.* **2012**, *3*, 445.
(15) Winter, M.; Besenhard, J. O.; Spahr, M. E.; Nóvak, P. *Adv. Mater.* **1998**, *10*, 725.
(16) Bonino, F.; Brutti, S.; Reale, P.; Scrosati, B.; Gherghel, L.; Wu, J.; Müllen, K. *Adv. Mater.* **2005**, *17*, 743.
(17) Caballero, A.; Hernán, L.; Morales, J. *ChemSusChem* **2011**, *4*, 658.
(18) Hassoun, J.; Lee, K. S.; Sun, Y. K.; Scrosati, B. *J. Am. Chem. Soc.* **2011**, *133*, 3139.
(19) Liu, N.; Hu, L.; McDowell, M. T.; Jackson, A.; Cui, Y. *ACS Nano* **2011**, *5*, 6487.
(20) Vargas, O.; Caballero, A.; Morales, J.; Elia, G. A.; Scrosati, B.; Hassoun, J. *Phys. Chem. Chem. Phys.* **2013**, *15*, 20444.
(21) Kim, T.-H.; Park, J.-S.; Chang, S. K.; Choi, S.; Ryu, J. H.; Song, H.-K. *Adv. Energy Mater.* **2012**, *2*, 860.
(22) Morales, J.; Trócoli, R.; Franger, S.; Santos-Peña, J. *Electrochim. Acta* **2010**, *55*, 3075.
(23) Zaghib, K.; Striebel, K.; Guerfi, A.; Shim, J.; Armand, M.; Gauthier, M. *Electrochim. Acta* **2004**, *50*, 263.
(24) Amine, K.; Liu, J.; Belharouak, I. *Electrochem. Commun.* **2005**, *7*, 669.
(25) Eshkenazi, V.; Peled, E.; Burstein, L.; Golodnitsky, D. *Solid State Ionics* **2004**, *170*, 83.
(26) Bryngelsson, H.; Stjerndahl, M.; Gustafsson, T.; Edström, K. *J. Power Sources* **2007**, *174*, 970.
(27) Zhang, S. S.; Xu, K.; Jow, T. R. *J. Power Sources* **2006**, *160*, 1349.
(28) Khai, T. V.; Na, H. G.; Kwak, D. S.; Kwon, Y. J.; Ham, H.; Shim, K. B.; Kim, H. W. *Carbon* **2012**, *50*, 3799.
(29) Li, S.-M.; Yang, S.-Y.; Wang, Y.-S.; Lien, C.-H.; Tien, H.-W.; Hsiao, S.-T.; Liao, W.-H.; Tsai, H.-P.; Chang, C.-L.; Ma, C-C. M.; Hu, C.-C. *Carbon* **2013**, *59*, 418.
(30) Lee, S.; Lim, S.; Lim, E.; Lee, K. K. *J. Phys. Chem. Solids* **2010**, *71*, 483.
(31) Chen, C.-M.; Huang, J.-Q.; Zhang, Q.; Gong, W.-Z.; Yang, Q.-H.; Wang, M.-Z.; Yang, Y.-G. *Carbon* **2012**, *50*, 659.
(32) Lee, J. T.; Nitta, N.; Benson, J.; Magasinski, A.; Fuller, T. F.; Yushin, G. *Carbon* **2013**, *52*, 388.
(33) Edström, K.; Herstedt, M.; Abraham, D. P. *J. Power Sources* **2006**, *153*, 380.
(34) Seel, J. A.; Dahn, J. R. *J. Electrochem. Soc.* **2000**, *147*, 892.
(35) Kang, S.-H.; Abraham, D. P.; Xiao, A.; Luncht, B. L. *J. Power Sources* **2008**, *175*, 526.
(36) Wu, Z.-S.; Xue, L.; Ren, W.; Li, F.; Wen, L.; Cheng, H.-M. *Adv. Funct. Mater.* **2012**, *22*, 3290.
(37) Aurbach, D.; Levi, M. D.; Levi, E.; Schechter, A. *J. Phys. Chem. B* **1997**, *101*, 2195.